The Solar Modulation Events of The 25^{th} Solar Activity Cycle as Seen by Particle Detectors' Networks

Chilingarian A.

A. Alikhanyan National Lab (Yerevan Physics Institute)

Corresponding author: **chili@aragats.am**

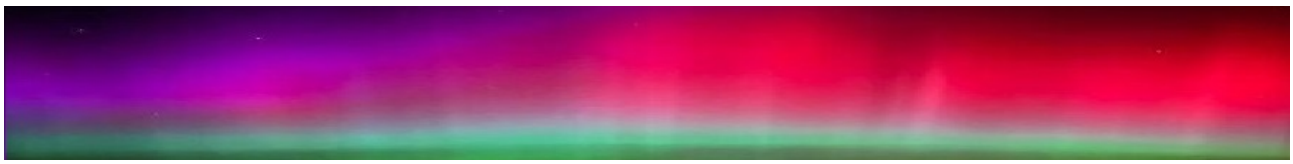

Abstract

Cosmic rays are direct messengers, conveying crucial information on solar-terrestrial relations. Networks of particle detectors continuously monitoring cosmic ray flux on the Earth's surface provide valuable insights complementary to spaceborne detectors operated by NOAA, NASA, and ESA. The ongoing deployment of new particle detectors at mountain altitudes, particularly spectrometers measuring energy release spectra of charged and neutral particles, is a strategic choice for understanding the cause of global count rate variations and their relation to the solar energetic particles (SEP) and intricate interactions between colliding magnetic fields. The energy spectra of particles reaching the detectors during violent solar events allow a direct comparison of the measured energy release spectrum with what is expected under different hypotheses on the type of solar event and SEP energy spectrum. The importance of using advanced measurement techniques of astroparticle physics to study solar-induced phenomena is underscored by the presented analysis of solar events of the 25th cycle. We apply the SEVAN network's spectrometers and developed spectra recovery techniques to characterize the Forbush decreases of 4 November 2011 and May 10, 2024, the magnetospheric effect of 5 November 2023, and the 74th GLE of May 11. We also formulate a refined definition of the magnetospheric effect to distinguish the magnetospheric effect from other solar events.

Keywords: GCR, SCR, Energy spectra, Forbush decrease, Magnetospheric effect, Ground-level enhancement

Introduction

The sun affects the Earth through electromagnetic radiation, plasma, and high-energy particles. Even though these particles' energy is a small fraction of visible light energy, they provide insights into fundamental particle acceleration processes [20]. They can also give timely information about space weather conditions that may impact space technologies and the Earth's environment [25].

The Earth has been bombarded by protons and fully stripped ions accelerated in the Galaxy for billions of years. This flow of particles may vary as the sun moves through the galactic arms in its orbit around the center of the Galaxy, influenced by nearby star explosions and changes in the geomagnetic field. Despite these fluctuations, the GeV galactic cosmic ray flux remains relatively stable over millions of years. On the other hand, our nearest star, the sun, is highly variable and can alter radiation and particle flux intensities by several orders of magnitude in just a few minutes. The most energetic flaring process re-

leases up to 10^{33} erg of energy in a few minutes [19]. Solar radiation significantly impacts the Earth, affecting climate, safety, and technological assets in space and on the surface.

The sun 'modulates' the low-energy Galactic Cosmic Rays (GCR) in several ways. Along with broadband electromagnetic radiation, the explosive flaring process usually results in the ejection of large amounts of solar plasma (coronal mass ejection – CME, [4]) and the acceleration of numerous electrons and ions (solar energetic particle event – SEP, [44]). Particles can be generated directly in the coronal flare site with subsequent escape into interplanetary space or accelerated in CME-associated shocks propagating through the corona and interplanetary space (becoming ICME, [32]). Accelerated charged particles and neutral ones, born in collisions with dense solar plasma, constitute the so-called solar cosmic rays (SCR, [21]). When these particles reach Earth's environment, they are detected by particle spectrometers on satellites and space stations. The highest energy particles generate extensive air showers (EASs, [1]) capable of reaching the Earth's surface and creating ground-level enhancements (GLEs, [42]).

Only a few Solar Energetic Particles (SEPs) provide enough energetic particles to be detected by surface particle detectors, and so far, only 74 Ground Level Enhancements (GLEs) have been recognized in nearly 80 years. The latitudinal dependence on the geomagnetic field (GMF) allows worldwide particle detectors to register Galactic Cosmic Rays (GCR) in the energy range defined by geomagnetic rigidities [46]. Depending on location, particle detectors are sensitive to different parts of the SEP spectra. Charged particles can enter the atmosphere with energies larger than a minimal value specific to geographical coordinates. The GMF redirects particles with smaller energies to lower altitudes or open space. The attenuation of particle cascades in the atmosphere also sets a threshold on the minimal energy of the primary particle. This effect is noticeable at geographical coordinates where the geomagnetic rigidity is minimal. The minimal energy of incoming cosmic rays at polar regions is determined by atmospheric rigidity, changing from approximately 300 MeV at high altitudes in Antarctica to 400 MeV for sea-level detectors in the same location [41]. The largest energy threshold of 17 GeV is attributed to equatorial sites, where the GMF is strongest. Practically, the minimal energies of registered particles are defined by the particle type, detector efficiency, data acquisition electronics, and the matter above the detector. Correcting the registered count rates according to the detector response function makes it possible to recover energy spectra within the accessible energy range. The GCR spectra can be approximated by the power law $\frac{dJ}{dE} \approx E^{-\gamma}$, where $\gamma \approx 2.7$. Solar Cosmic Ray (SCR) flux at GeV energies is usually very weak ($\gamma > 7$); only in some exceptional solar events, such as in 1956 and 2005, were the spectra of SCR considered "hard" ($\gamma \approx 4 - 5$) at the highest energies [3]. The "hard" spectra in solar events emphasize the necessity for alertness and readiness, as numerous mid-level energy particles (50-100 MeV) arriving within minutes during such events can cause significant damage to satellite electronics.

Cosmic rays are monitored on Earth by several networks of particle detectors, which measure secondary cosmic rays produced when primary protons and stripped nuclei interact with atmospheric atoms. These networks include the Neutron Monitor network (NM, [45, 34]), the Solar Neutron Telescope (SNT) network [39], the SEVAN network [11], which additionally captures electron, gamma ray, and muon fluxes, Spaceship Earth [31], and the Global Muon Detector Network (GMDN, [37]). The network of NMs covers almost the whole globe, from the Antarctic to the Arctic regions; flux intensities measured at different sites can be accessed from the NM database (NMDB, [33]). SEVAN network detectors are located at mountain tops in Armenia, Germany, and Eastern Europe; other networks are located at different latitudes and longitudes. Neutron monitors and SEVAN networks detect solar events surprisingly coherently [29].

Other solar modulation effects also influence the intensity of cosmic rays. The solar wind "blows out" the lowest energy GCR from the solar system, thus changing the GCR flux intensity depending on the solar cycle year. Huge magnetized plasma clouds and shocks initiated by CMEs travel in interplanetary space with velocities up to 2000 km/s and disturb the interplanetary magnetic field (IMF). When these disturbances reach the magnetosphere, they introduce anisotropy in the GCR flux near Earth, creating depletion and enhancement regions. The size and occurrence of the southward component of IMF (B_z) correlate with the modulation effects ICME poses on the ambient population of the galactic cosmic rays during its propagation to the Earth [8]. Upon arrival at the magnetosphere, the overall depletion of the GCR triggered by the interplanetary shock and plasma cloud manifests itself as a decrease in the secondary cosmic rays detected by the networks of particle detectors on the Earth's surface (Forbush decrease, [24]). The abrupt change in the geomagnetic field, known as sudden storm commencement (SSC, [47]), leads to the main decrease phase caused by the southward magnetic field.

The relative decrease of the count rate at the particle monitors is well pronounced at high latitudes. Due to low magnetic cutoff rigidity at high latitudes, the primary protons and ions, responsible for the greater part of the count rate, have considerably low energy (< 1 GeV). Therefore, the count rate of these monitors is strongly depleted by the disturbances of the IMF. The count rates of particle monitors at mid-

dle to low latitudes are formed by the primaries with energies much higher (> 5 GeV). Therefore, the depletion of the count rates of these monitors will be less compared to high-latitude monitors. In turn, geomagnetic storms (GMS, [11]), appearing as a sudden change in the Earth's magnetic field, can magnify the relative change of the count rates of middle and low-latitude particle detectors without any corresponding notable alteration in the count rates of the high-latitude detectors [22]. If the magnetic field of ICME is directed southwards, it reduces the cutoff rigidity, originating the so-called magnetospheric effect (ME, [30]). Low-energy GCRs, usually effectively declined by the magnetosphere, penetrate the atmosphere and generate additional secondary particles, thus enlarging the count rate of the monitors located at middle and low latitudes. At high latitudes, where cutoff rigidity is very low, the count rates of particle detectors are determined mostly by the atmospheric cutoff, which doesn't depend on GMS. The decrease in the geomagnetic cutoff does not affect the number of secondary particles reaching the detectors at high latitudes.

With the primary goal of measuring solar events, the SEVAN network is also used to research enhanced particle fluxes of atmospheric origin, so-called thunderstorm ground enhancements (TGEs, [9]). Observations of particle fluxes from thunderous atmosphere discover electron accelerators operating in thunderclouds. The particle avalanches from electron accelerators, possessing energies of tens of MeV, cover vast atmospheric volumes and expansive areas on Earth's surface. The ionosphere influences the atmospheric electric fields that initiate electron accelerators. Thus, revealing the possible link between TGEs and magnetospheric-ionospheric disturbances caused by ICMEs is another research goal of the SEVAN network. Appropriate facilities for measuring geomagnetic and electric field disturbances have been operated on Aragats for 15 years [15].

At high latitudes, where abundant low-energy primaries produce secondary particles, the flux enhancement during GLEs can reach 1000%; at middle-low latitudes, the enhancements due to SCR are much smaller, usually not more than 2-5%. For energies greater than 10 GeV, the intensity of the GCR becomes increasingly higher than the intensity of the largest known SEP events (see Fig. 1 of [18]), and we confront a very complicated problem of detecting a small signal of the SCR against the huge "background" of the GCR. Low statistics experiments can sometimes demonstrate fake peaks with high significance. Some remedies to avoid erroneous inference on signal existence at low statistics are discussed in [10].

An alternative way to recover energy spectra is to measure different types of particles at the same place. For instance, neutrons and muons [2], or neutrons, muons, electrons, and gamma rays [5]. Or using particle intensities measured at the same geographical coordinates but at altitudes, having various effective atmospheric cutoff rigidities [18]. In this way, using intensities measured by particle detectors on slopes of Mt. Aragats, the spectral index of the 20 January 2005 GLE was estimated [50]. The same paper investigated the relation of the measured secondary particle energy spectra to the primary SCR energy spectra. The most probable energies of primaries originated secondaries with definite energy thresholds were estimated. However, during the 23rd solar activity cycle, the Aragats Space Environmental Center (ASEC, [6]) missed appropriate spectrometers and spectra recovery methods. With the rise of solar activity in the maximum of the 25th cycle, ASEC was already equipped with various spectrometers [12] and appropriate methods for solving the inverse problem of CR [16]. In the next sections, we will describe new facilities and apply new methods for analyzing solar events of the 25th solar activity cycle.

SEVAN detector

The basic detector of the SEVAN network (Figure 1a, see [7]) consists of assemblies of standard slabs of $50 \times 50 \times 5\,\mathrm{cm}^3$ plastic scintillators. Two identical $100\times100\times5\,\mathrm{cm}^3$ scintillators and two $100\times100\times5\,\mathrm{cm}^3$ lead filters are positioned above and below a thick $50 \times 50 \times 25\,\mathrm{cm}^3$ scintillator stack. Scintillator light capture cones, and PMTs are located on the detector's top, bottom, and intermediate layers. The total weight of the SEVAN detector, including the steel frame and detector housings, is approximately 1.5 tons.

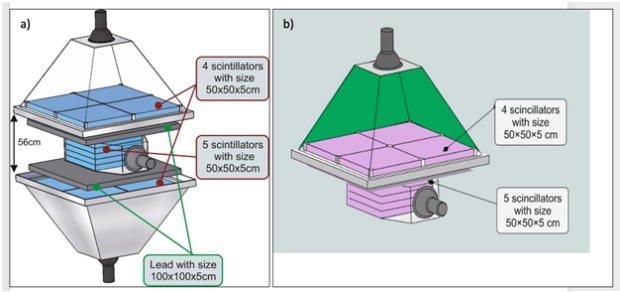

Figure 1: Basic SEVAN detector(1a) and SEVAN-light detector (1b)

In April 2023, we installed a modernized SEVAN-light detector at the Umwelt-Forschungs-Station (UFS, Schneefernerhaus, 2650 m asl, see Fig. 1b) near the top of the Zugspitze (2962 m), a site with a long history of atmospheric research, where Joachim Kuettner conducted his seminal experiments on the structure of the electric field in the lower atmosphere. Due to building constraints at UFS, SEVAN-light needed to be compact, shorter, and much lighter than the basic SEVAN. Thus, SEVAN-light consists of only 2

layers, and the lead absorber is not included (total weight ≈100 kg). However, we added a modernized electronics board with a logarithmic amplitude-to-digit-converter (LADC), which provides particle energy spectrum recovery in the 7–100 MeV range. This feature allows for measuring the energy spectrum of the GLE and ME particles [16] and missing particles during FD. The SEVAN-light is also fully operational for high-energy atmospheric physics research, with the additional feature of measuring the energy spectrum of TGE particles.

Data Acquisition (DAQ) electronics provide registration and storage of all coincidences of the detector signals for further offline analysis and for issuing online alerts, thus allowing the registration of neutral and charged particles and high-energy muons. Table 1 presents the purity of the SEVAN-light flux observed by different coincidences of the detector operation. If we denote by "1" the signal from a scintillator and by "0" the absence of a signal, the "01" coincidence efficiently selects neutrons (≈32%) and gamma rays (≈64%), while the "11" coincidence selects muons (63%) and electrons (23%).

The next sections will demonstrate how the newly introduced experimental facilities can be used for analyzing solar events: Forbush decreases, Magnetospheric effects, and Ground-level enhancements.

Forbush Decrease measured by the SEVAN network on November 4, 2021.

On 3–5 November 2021, a large GMS unleashed auroras as far south as the low latitude of New Mexico (39° N). SOHO coronagraphs captured the storm cloud leaving the Sun on November 2, following and overtaking a previous slower-moving solar flare (M1.7) in the magnetic canopy of sunspot AR2891. As the "cannibal" ICME approached and passed the satellites at the L1 point on 4 November, the IMF reached large values, approaching and exceeding 20 nT (Fig. 2a); the B_z component of the IMF dipped to -15 nT at 8:00 UT and then turned to the positive domain afterward (Fig. 2b). The geomagnetic field measured at the Aragats station by the LEMI-417 sensor changed coherently, reaching a minimum at approximately 11:08 (Fig. 2c); the B_x component, after large disturbances, also reached a minimum (compressed by the solar wind) at approximately 11:09 (Fig. 2d). Thus, the depletion phase of FD, outlined in Fig. 2 by red lines, coincides with the largest values of IMF, fast-changing values of B_z, and compression of the magnetosphere (lowest values of the geomagnetic field and its B_x component).

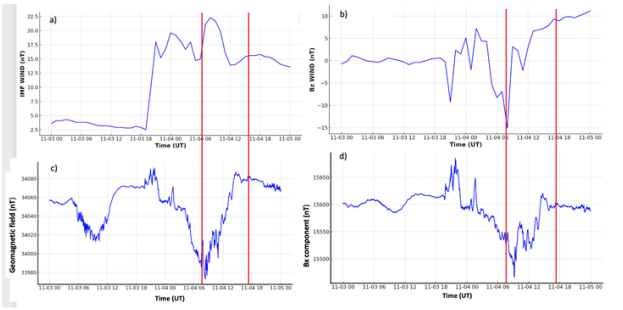

Figure 2: a) Scalar IMF B; b) IMF Bz component; c) and d) geomagnetic field and its Bx component. Red lines show the depletion phase of FD.

In Fig. 3, we show the FD detection with the SEVAN network. The FD started with a significant pre-FD increase, which lasted nearly 4.5 hours from 6:00 to 10:00 on Aragats and nearly 4 hours from 6:30 to 10:30 on Lomnicky Stit (see Fig. 3). Although the amplitude of FD is larger in neutron data, the shape and timing of FD are coherent for neutron and muon fluxes (for details of SEVAN detector operation, see the instrumentation section of [14]).

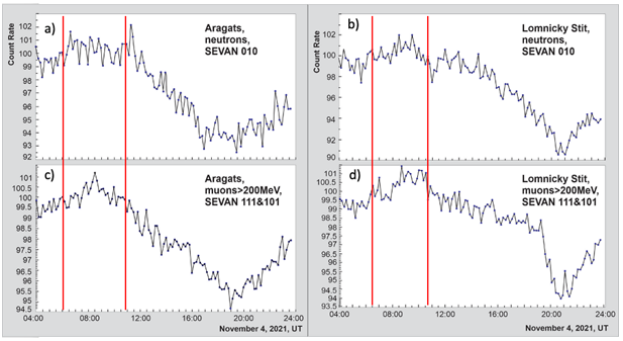

Figure 3: Ten-minute time series of count rates measured at Aragats and Lomnicky Stit by the SEVAN "111 + 101" coincidences selected muons with energies > 200 MeV. Red lines show the pre-FDs registered at both stations.

Mountain SEVAN detectors coherently registered a pre-FD increase in fluxes of high-energy muons (E_μ > 200 MeV, SEVAN coincidence "111 & 101", muons traversing 10 cm of lead). After the pre-FD, the SEVAN network registered the FD main phase on Aragats, Lomnicky Stit, Mileshovka, and Hamburg. Figure 4 shows the FD in a 1-minute time series of count rates of the "010" coincidence (mostly neutrons). The FDs at mountain altitudes (Aragats, Lomnicky Stit, all above 2500 m, Figs. 4a and 4b) are more pronounced than at lower altitudes (Mileshovka, ≈800 m, Fig. 4c) and sea level (Hamburg, Fig. 4d).

SEVAN-light	Neutron (%)	Proton (%)	mu+ (%)	mu- (%)	e- (%)	e+ (%)	gamma ray (%)
Coin. "01" (neutral)	32.1	0.3	1.0	0.9	1.0	0.9	63.8
Coin. "11" (charged)	1.6	6.4	33.3	29.6	12.1	10.4	6.5

Table 1: The share of cosmic ray species selected by different coincidences of the SEVAN-light detector in percent.

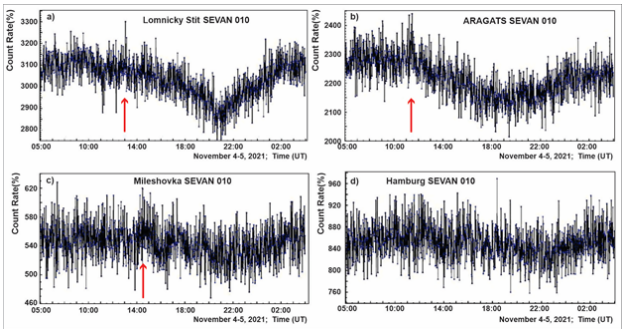

Figure 4: Pressure-corrected 1-minute time series of count rates of "010" coincidence of SEVAN (primarily neutrons). We show the "pre-Forbush" count rate enhancement by red arrows followed by FD at high-altitude detectors (not seen at sea level).

In Figure 5, we compare the FD registration by the Neutron Monitor and the "010" coincidence of the SEVAN detector, located in the same place at Lomnicky Stit. The correlation of both is perfect, although the FD amplitude measured by the Neutron Monitor (NM) is larger than that of SEVAN.

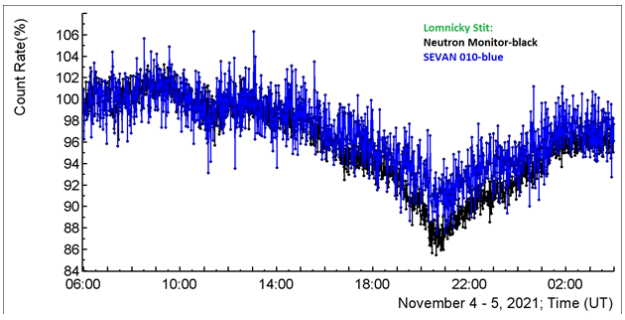

Figure 5: 1-minute time series of count rates of Neutron Monitor (black) and SEVAN's "010" (primarily neutrons) coincidence, both located at Lomnicky Stit.

Magnetospheric event on 5 November 2023

The first feature of the magnetospheric effect is the absence of enhancements at Antarctic NMs. Fig. 6 shows the time series from several high-latitude NMs, showing no enhancement. Only the DRBS monitor shows an apparent enhancement. However, it is not in Antarctica but in the Geophysical Center of Dourbes (Belgium); see also Fig. 1 of [28].

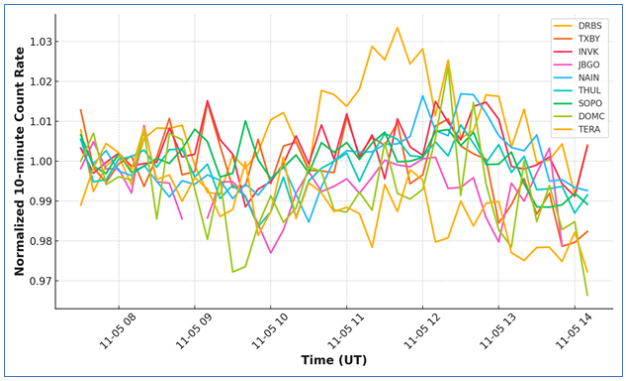

Figure 6: Normalized 10-minute time series of the Antarctic, near-polar, and Belgium neutron monitors during the solar event of 5 November 2023.

In Fig. 7, we show correlated enhancements (3–4%) in count rates at middle latitudes and high-altitude NMs. The time series are measured by NMs across more than 5500 km. The shapes of the enhancements are similar, and the correlations are obvious. In contrast, monitors located at sea level do not show enhancements due to the attenuation of the neutron flux in the thick air, caused by atmospheric cutoff (see Figs. 5 and 6 of [17]).

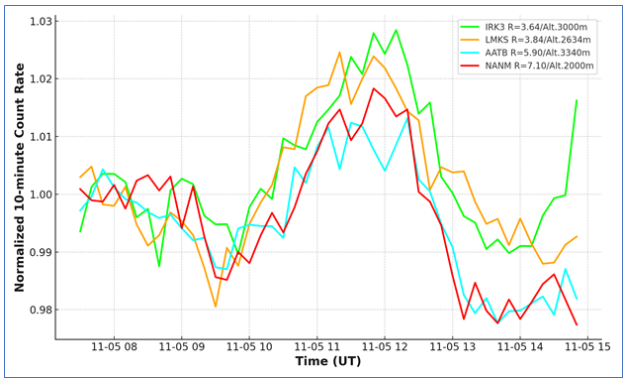

Figure 7: Pronounced enhancement in the count rates of NMs located at middle latitudes and high altitudes.

Fig. 8a shows the scatter plots between the Antarctic NM Terre Adelie and the South Pole; the correlation is only 0.31. For the middle-latitude NMs Irkutsk3 in Siberia, RF, and Lomnicky Stit in Slovakia (distance 5500 km), the correlation coefficient is 0.81 (Fig. 8b).

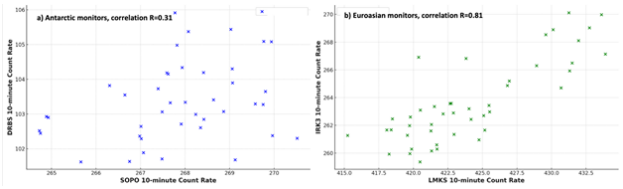

Figure 8: a) Scatter plots between count rates of Antarctic NMs; b) the same for middle latitude Euroasian NMs.

In Fig. 9a, we compare the count rates of the SEVAN detector's "100" coincidence – signal only in the upper scintillator. The count rate dynamics of both detectors, located at a distance of ≈2000 km, are very similar, and the correlation coefficient, shown in Fig. 9b, is 0.6. The ME enhancement reaches 2–2.5%, which is smaller than for neutron monitors. The "100" coincidence selected charged particles with energies above 5 MeV. Thus, the count rate of the Aragats SEVAN, located 500 m above Lomnicky Stit, is higher.

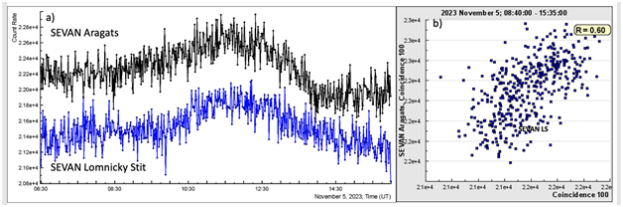

Figure 9: a) 1-minute time series of the "100" coincidence of SEVAN detector on Aragats and Lomnicky Stit; b) scatter plot between count rates of SEVAN detectors.

Observation of the solar events by the SEVAN network during Geomagnetic disturbances on May 10-11

The 25th solar activity cycle, the maximum of which is expected in 2024, has already produced a series of interplanetary coronal mass ejections (ICMEs), solar energetic particles (SEPs), and solar particle events detected both in space and on the Earth's surface. The G5 geomagnetic storm that occurred on May 10–11, 2024, was one of the most intense in over two decades (see detailed analysis of the event in [26]). This event led to a significant Forbush decrease (FD), accompanied by Ground Level Enhancement (GLE) #74 in its recovery phase. Ground-based neutron monitors [33] confirmed a GLE from 02:00 UT on 11 May 2024, following an X5.8-class solar flare that reached its maximum at 01:23 UT.

In Fig. 10, we show the disturbances of the X-component of the geomagnetic field (GMF) measured by the Aragats magnetometer (blue), along with the SEVAN-light count rate (red) and disturbances of the near-surface electric field (black). The electric field during solar events was quiet: no thunderstorms and lightning flashes were detected. The Aragats magnetometer observed a storm sudden commencement (SSC) at 17:05, which triggered the extreme geomagnetic storm with a Dst index of −412 nT at 2 UT on 11 May 2024, marking the sixth-largest storm since 1957. The magnetometer also shows a large compression upon the shock arrival, confirmed by THEMIS-E's and Kakioka's measurements on the magnetic field and plasma data [26].

The atmospheric electric field was calm during major geomagnetic disturbances. However, it is interesting to note that 3 hours before SSC, at 14:00, the count rate experienced an abrupt burst (TGE, [9]) due to an enhanced flux of electrons and gamma rays of atmospheric origin (see the peak in the black curve at the left bottom corner).

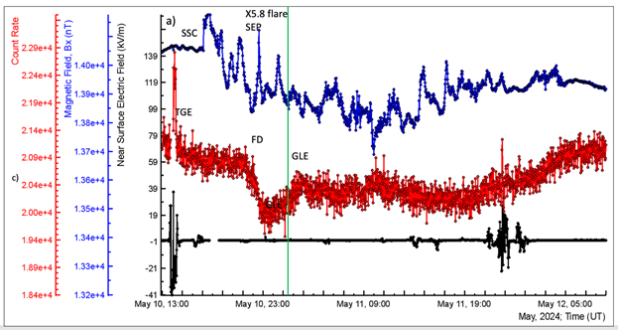

Figure 10: The X-component of the GMF measured by the Aragats magnetometer (blue), along with disturbances of the near-surface electric field (black) and the count rate of the SEVAN-light detector (red).

In Fig. 11, we present a 10-minute time series of count rates of the Nor Amberd neutron monitor (NANM) and neutral and charged fluxes selected by the coincidences of the SEVAN-light detector. Depletion of fluxes was calculated according to the mean values measured from 19:00 to 20:00 on May 10 (shown by the dashed lines). The FD started at ≈18:30, approximately 1.5 hours after the SSC. As mentioned in [43], "when ICME with depleted cosmic ray flux inside passes over the Earth, ground-based monitors generally show a decrease in their flux." Maximum depletion was ≈8% for the NANM and ≈5% for SEVAN-light, reached around midnight. Subsequently, during the recovery phase, the FD was interrupted by a GLE after the X5.8 flare unleashed the SEP. The GLE amplitude was calculated relative to the mean values measured from 23:00 to 24:00 on May 10.

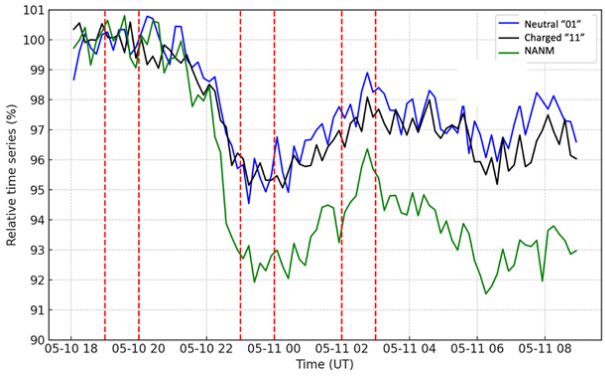

Figure 11: Time series of count rates of Nor Amberd Neutron Monitor (NANM, green) and SEVAN-light neutral and charged particles (blue and black).

Figure 12 shows a minute-by-minute time series of precise correlated counts from the 5 cm thick, 1 m^2 area SEVAN upper scintillators on Mts. Aragats (40.25° N, 44.15° E, altitude 3200 m), Musala (42.1° N, 23.35° E, altitude 2930 m), and Lomnicky Stit (49.2° N, 20.22° E, altitude 2634 m).

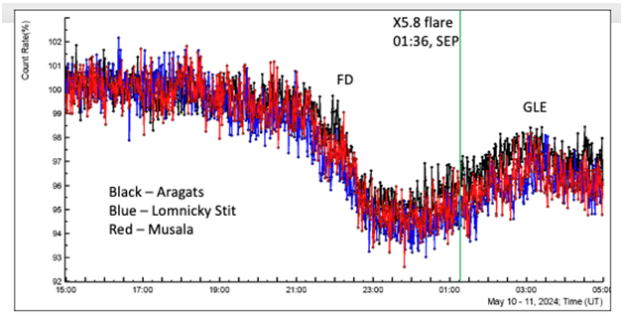

Figure 12: Observation of FD and GLE by SEVAN network's Aragats, Lomnicky Stit, and Musala detectors.

The NM multiplicity as a measure of variations in particle flux arriving at the Earth

A technique has recently been proposed for accessing variations in the spectra of GCR [36] during solar events. Modified electronics of neutron monitors (NM) collect all thermal neutrons with precise timestamps of their arrival. Measuring time spans between successive thermal neutron counts can be used to calculate neutron multiplicity, i.e., the number of thermal neutrons corresponding to the high-energy hadron hitting the NM. Multiplicity relates to the energy of secondaries from cosmic-ray showers and, consequently, to the primary cosmic-ray energy.

The Aragats neutron monitor (ArNM) consists of 18 gas-filled cylindrical proportional counters of CHM-15 type (length 200 cm, diameter 15 cm) enriched with boron trifluoride ($^{10}BF_3$). ArNM is grouped into 3 sections organized in a line, each consisting of 8 proportional chambers. The proportional counters are surrounded by a 5 cm thick lead cover and a 2 cm thick layer of polyethylene. The cross-section of the lead above each section has an area of 6 m^2, and the total surface area of the three sections is 18 m^2. High-energy hadrons produce multiple thermal neutrons in the lead. Then, neutrons enter the sensitive volume of the proportional counter and yield Li^7 and α particles via interactions with boron trifluoride [35]. The α particle accelerates in the high electric field inside the proportional counter and produces a pulse registered by the data acquisition electronics. If all pulses need to be counted, the dead time of the NM should be kept very small. If only the incident hadrons must be counted (a one-to-one relationship between count rate and hadron flux), the dead time must match the secondary neutron collection time (≈1250 μs) to avoid double-counting.

For the first time in [49], the detection of neutron bursts (high multiplicity events) in the NM related to the occasional hitting of the detector by a core of a high-energy extensive air shower (EAS) was described. This option of EAS core detection by NM was almost not recognized in the past because the commonly used long dead time does not permit counting the neutron multiplicity. By establishing a 3000 times shorter dead time of 0.4 μs, ArNM detects EASs hitting ArNM, several of which provide bursts with a neutron multiplicity exceeding 2000 (see Figs. 20–22 of [13]). The primary particle energies corresponding to these events are very high (> 10 PeV).

ArNM signals were monitored with a high-frequency digitizing oscilloscope to observe the neutron burst in more detail. Signals from the ArNM were relayed to the MyRIO board (National Instruments), which produced a pulse for oscilloscope triggering when the count rate of the detector exceeded a preset threshold value (usually a 20% enhancement above the running average). The sequence of pulses from proportional counter N2 of the ArNM recorded by a Picoscope 5244B is shown in Fig. 13 (for better visibility, pulses were inverted). The record length was 100 milliseconds, including 20 milliseconds pre-trigger time (denoted with a minus sign) and 80 milliseconds post-trigger time. The sampling rate was 250 Mb/s, corresponding to a sampling interval of 4 ns, and the amplitude resolution was 8 bits. Bursts were observed as sequences of microsecond pulses temporally isolated from other pulses on a time scale of at least 100 microseconds.

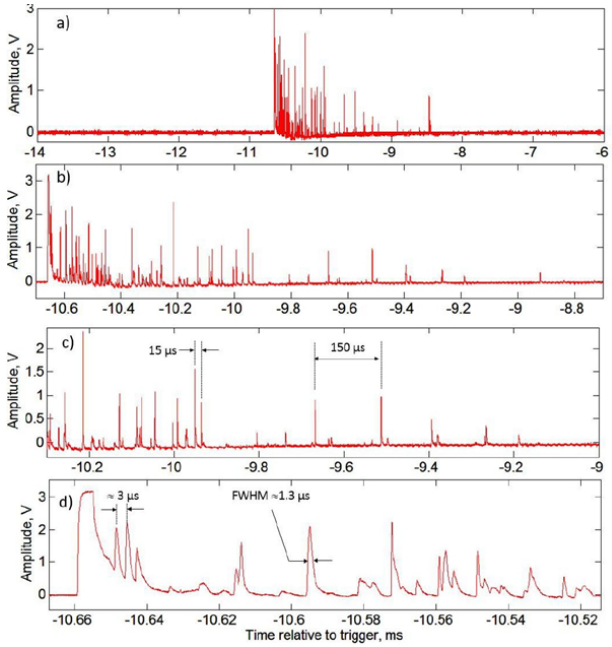

Figure 13: The oscilloscope recorded a neutron burst that occurred at 4:08:05 on November 26, 2016. The burst duration is ≈ 2.2 milliseconds, and the multiplicity is 107 per m^2. The four panels (a–c) show the burst records on different time scales.

Fig. 14 (also inverted) shows the typical single signal shape. The observed burst is rather "dense" at the beginning (the interval between pulses is a few microseconds) and becomes much sparser at the end (the interval between pulses ranges from tens to hundreds of microseconds). The pulse amplitude is largest at the beginning of a burst most frequently. The interval between pulses varies during the burst: it is the shortest (about 3–5 μs) at the beginning and increases to tens and hundreds of microseconds toward the end of the burst. The rise time of the neutron signal is ≈300 ns, and the duration is ≈500 ns.

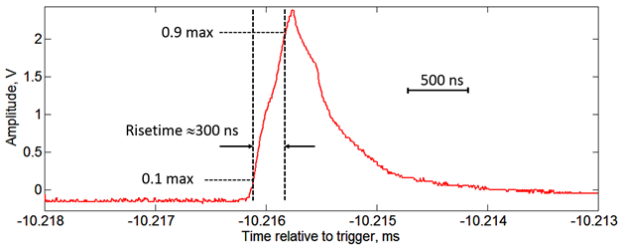

Figure 14: A 5-μs fragment of the oscilloscope record shows a typical pulse shape of the neutron monitor; the rise time (0.1–0.9) is approximately 300 ns.

Exhaustive information on EAS core hitting ArNM can be found in the dataset of 50 high-multiplicity events published in the Mendeley repository [48]. In Fig. 15a, we show the distribution of neutron burst durations for 50 selected events from the Mendeley dataset; in Fig. 15b, the distribution of the multiplicities of these events registered by the proportional counter of the ArNM.

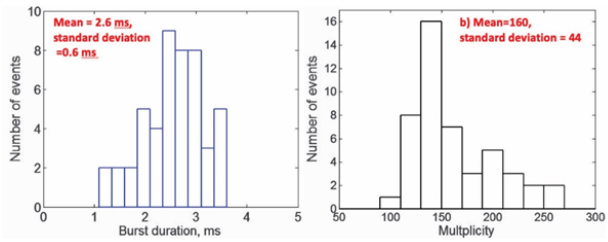

Figure 15: Histogram of the neutron burst duration (a) and corresponding multiplicity histogram (b).

The frequency and amplitude of thermal neutron bursts registered by NM (neutron multiplicities) can be used to track variations of the GeV-range protons incident in the terrestrial atmosphere. A hard solar proton spectrum during GLE will induce more neutron bursts, and the multiplicity will grow. Analogously, large magnetospheric disturbances leading to FD will induce more traps for GeV energy GCR, and the frequency of neutron bursts will reduce (lower multiplicity).

Technically, it is difficult to count millisecond-length neutron bursts. ArNM DAQ electronics presents NM data as a one-second time series, and the second containing an NM burst can be easily outlined and digitized. For Aragats cutoff rigidity (7 GV), the probability that two neutron bursts occur in a particular second is negligibly small, and the multiplicity can be estimated by subtracting the mean count rate from the count rate measured in a high-multiplicity second.

We tested the multiplicity analysis with all types of solar events described in the paper. Fig. 16 shows a 1-hour time series of multiplicities measured during an ME (a), FD (b), GLE (c), and a sample related to the quiet Sun period (d). Solar events do not influence multiplicity distributions; the mean values, variances, and relative errors are approximately the same for all three types of solar events and for quiet time. Possibly, only in the Antarctic region with very low cutoff rigidity is the "Leader fraction" approach justified [36].

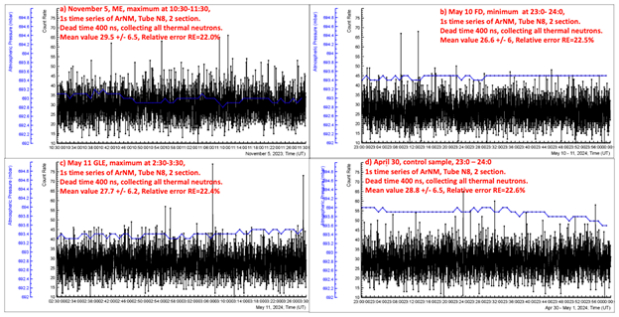

Figure 16: 1s time series of multiplicities measured during three types of solar events (a-c) and quit time (d).

Therefore, in the next section, we describe another method for estimating the energy release histograms of neutral and charged particles measured during solar events.

The energy spectra of the ME event on 5 November 2023 and the GLE event on May 11, 2024

Fig. 17 shows the energy spectra of neutral particles measured by the SEVAN-light spectrometer. See details of detector operation in [16] and spectrum recovery methods in [12]. The measured energy spectrum of the "additional particles" on 5 November 2023 is limited by 10 MeV, indicating low-energy primaries giving rise to this ME event. The storm-induced weakening of the geomagnetic shielding allows primary GCR with energies below geomagnetic cutoff rigidity to enter the atmosphere and originate EASs. In contrast, the secondaries from SEP on May 11 (see details on the GLE event in [26] and [14]) extend up to 100 MeV (Fig. 17b). As demonstrated in [3, 11], the energies of solar protons can reach 20 GeV and higher. Thus, SCR can generate secondaries with much larger energies than GCR below the geomagnetic cutoff during magnetospheric effects (less than 7 GeV).

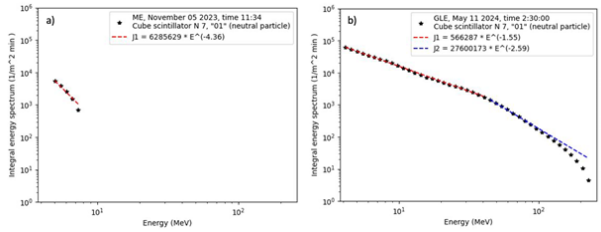

Figure 17: The integral energy spectra of ME particles a), and GLE particles b) measured by the spectrometer on Aragats.

The GCRs comprising additional particles on 5 November 2023 have lower energies than geomagnetic rigidity. Therefore, they produce lower-energy secondaries due to atmospheric rigidity, reaching only mountain altitudes, not sea level. Consequently, there should not be flux enhancement at sea level monitors. We demonstrate how atmospheric rigidity works in Fig. 18, where we show the energy spectra of secondary electrons and gamma rays produced by 7 GeV protons entering the atmosphere above the Aragats mountain.

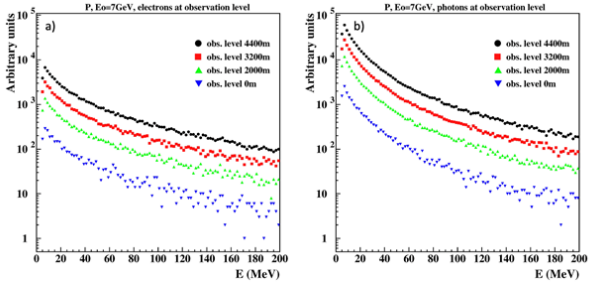

Figure 18: Energy spectra of secondary electrons a) and gamma rays b) from the EASs originated by a primary proton with energy 7 GeV, depending on the height of the observation level.

To obtain fluxes of secondary particles, we use the CORSIKA code [27] version 7.75, simulating EASs with the hadronic interaction models QGSII_UrQMD [23], along with the electromagnetic interaction model EGS4 [40]. Protons with 7 GeV energy enter the terrestrial atmosphere vertically. We tracked shower electrons/positrons and gamma rays until they reached an energy of 5 MeV, and muons until 10 MeV, executing 1,000,000 simulation trials. Table 2 shows a low likelihood of detecting secondary particles from 7 GeV protons. Consequently, these particles cannot reach sea level, making them undetectable by neutron monitors and scintillators at sea level. During a Ground Level Enhancement (GLE) event, solar protons generate secondary particles with energies that surpass the cutoff rigidity. These high-energy protons produce secondary particles that reach sea level, where ground-based detectors can detect them.

Obs. Level (m)	μ^+ & μ^-	e^+ & e^-	γ
0	0.011	0.003	0.018
2000	0.032	0.016	0.090
3200	0.054	0.040	0.218
4400	0.084	0.086	0.468

Table 2: Number of secondary particles per primary proton at different observation levels.

Conclusion

The unexpected surge in solar activity in the fall of 2023, following the relatively calm 24th solar cycle, suggests the approach of the solar maximum of the

25th cycle in October 2024. The nonlinear interactions between interplanetary and geomagnetic fields result in diverse effects, ranging from severe geomagnetic storms (GMS) to spectacular auroras. In this context, understanding solar activity's impact on Earth's environment becomes increasingly critical.

One of the key issues in assessing the potential damage from solar cosmic rays to satellites and terrestrial technologies is the "hardness" of the solar energetic particle (SEP) energy spectrum. When the spectral index of SEPs at GeV energies is in the range of 5–6, abundant protons in the 50–100 MeV range pose a serious threat to satellite electronics. We tested several methods to assess the energy spectra of solar protons. The most promising approach involves measuring the energy release histograms of secondary cosmic rays, reconstructing their energy spectra, and correlating them with the primary SEP energies.

Using the SEVAN-light detector, we measure the energy releases of neutral and charged particle fluxes during ground-level enhancement (GLE) and magnetospheric effect (ME) events. The notable differences in the energy release patterns between these two event types confirm the sensitivity of our proposed method for assessing SEP energy spectra.

Our proposed method can also be valuable for analyzing Forbush decreases, offering insights into the movement of the so-called GCR barrier [38].

We also propose a refined definition of the Magnetospheric Effect (ME). Our classification consists of the following criteria:

1. **Observation by High-Latitude and Middle-Latitude Detectors**: Antarctic and near-polar neutron monitors do not register flux enhancements, whereas middle-latitude NMs and muon detectors consistently observe count rate increases.

2. **Influence of Atmospheric Cutoff Rigidity**: Due to atmospheric cutoff rigidity, NMs and SEVAN detectors located on mountain tops at middle latitudes exhibit flux enhancements, while those at sea level do not.

3. **Distinct Energy Spectra**: The energy spectra of shower particles measured during ME events differ significantly from other causes of flux enhancement, making this criterion essential for ME identification.

Acknowledgments

We thank our colleagues from the Neutron Monitor Database (NMDB) collaboration for engaging in valuable discussions. We also acknowledge the NMDB database (www.nmdb.eu), established under the European Union's FP7 program (contract No. 213007), for providing access to neutron monitor data.

Data Availability Statement

The data supporting this study's findings are available at http://adei.crd.yerphi.am/.

References

[1] Auger, P., Ehrenfest, P., Maze, R., Daudin, J., and Fréon, R. A. Extensive cosmic-ray showers. *Rev. Mod. Phys. 11* (Jul 1939), 288–291.

[2] Blanco, J. J., Sindulfo Ayuso, S., Regadío, A., et al. Evolution of the cosmic ray spectrum during a forbush decrease. *Advances in Space Research 73* (2024), 4842.

[3] Bostanjyan, N., Chilingarian, A., Eganov, V., and Karapetyan, G. On the production of highest energy solar protons at 20 january 2005. *Advances in Space Research 39*, 9 (2007), 1454–1457.

[4] Cane, H. V., and Lario, D. An Introduction to CMEs and Energetic Particles. *Space Science Reviews 123*, 1-3 (Mar. 2006), 45–56.

[5] Chilingarian, A., Arakelyan, K., Avakyan, K., et al. Correlated measurements of secondary cosmic ray fluxes by the aragats space-environmental center monitors. *Nuclear Instruments and Methods in Physics Research Section A 543* (2005), 483.

[6] Chilingarian, A., Babayan, V., Bostandjyan, N., et al. Monitoring and forecasting geomagnetic and radiation storms during the 23rd solar cycle: Aragats regional space weather center. *Advances in Space Research 31* (2003), 861–865.

[7] Chilingarian, A., Babayan, V., Karapetyan, T., et al. The sevan worldwide network of particle detectors: 10 years of operation. *Advances in Space Research 61* (2018), 2680–2696.

[8] Chilingarian, A., and Bostanjyan, N. On the relation of the forbush decreases detected by asec monitors during the 23rd solar activity cycle with icme parameters. *Advances in Space Research 45* (2010), 614–621.

[9] Chilingarian, A., Daryan, A., Arakelyan, K., et al. Ground-based observations of thunderstorm-correlated fluxes of high-energy electrons, gamma rays, and neutrons. *Physical Review D 82* (2010), 043009.

[10] Chilingarian, A., and Hovsepyan, G. Proving "new physics" by measuring cosmic ray fluxes. *Astronomy and Computing 44* (2023), 100714.

[11] Chilingarian, A., Hovsepyan, G., Arakelyan, K., et al. Space environmental viewing and analysis network (sevan). *Earth, Moon, and Planets 104* (2009), 195–210.

[12] Chilingarian, A., Hovsepyan, G., Karapetyan, T., et al. Measurements of energy spectra of relativistic electrons and gamma-rays avalanches developed in the thunderous atmosphere with aragats solar neutron telescope. *Journal of Instrumentation 17* (2022), P03002.

[13] Chilingarian, A., Hovsepyan, G., and Kozliner, L. Extensive air showers, lightning, and thunderstorm ground enhancements. *Astroparticle Physics 82* (2016), 21.

[14] Chilingarian, A., Karapetyan, T., Sargsyan, B., Asatryan, K., and Gabaryan, G. Influence of magnetosphere disturbances on particle fluxes measured by ground-based detector. *EPL 148* (2024), 19001.

[15] Chilingarian, A., Karapetyan, T., Sargsyan, B., Khanikyanc, Y., and Chilingaryan, S. Measurements of particle fluxes, electric fields, and lightning occurrences at the aragats space-environmental center (asec). *Pure and Applied Geophysics 181* (2024), 1963.

[16] Chilingarian, A., Karapetyan, T., Sargsyan, B., Knapp, J., Walter, M., and Rehm, T. Energy spectra of the first tge observed on zugspitze by the sevan light detector compared with the energetic tge observed on aragats. *Astroparticle Physics 156* (2024), 02924.

[17] Chilingarian, A., Karapetyan, T., Sargsyan, B., Knapp, J., Walter, M., and Rehm, T. Increase in the count rates of ground-based cosmic-ray detectors caused by the heliomagnetic disturbance on 5 november 2023. *EPL 148* (2024), 19001.

[18] Chilingarian, A., and Reymers, A. Particle detectors in solar physics and space weather research. *Astroparticle Physics 27* (2007), 465.

[19] Cliver, Edward W., and Dietrich, William F. The 1859 space weather event revisited: limits of extreme activity. *J. Space Weather Space Clim. 3* (2013), A31.

[20] Dorman, L. I. *Comsic rays. Variations and space explorations.* 1974.

[21] Dorman, L. I., and Venkatesan, D. Solar cosmic rays. *Space Science Reviews 64* (1993), 183–362.

[22] Dvornikov, V. M., Sdobnov, V. E., and Sergeev, A. V. Anomalous variations of cosmic rays in the rigidity range of 2–5 gv and their connection with heliospheric disturbances. *Izvestiya Akademii Nauk, Seriya Fizicheskaya (USSR) 52*, 12 (1988). All-Union Conference on Cosmic Rays, Alma-Ata (USSR), 13-15 Sep 1988.

[23] Fesefeldt, H. The simulation of hadronic showers - physics and applications. Technical Report PITHA-85/02, RWTH Aachen University, 1985.

[24] Forbush, S. E., Gill, P. S., and Vallarta, M. S. On the mechanism of sudden increases of cosmic radiation associated with solar flares. *Rev. Mod. Phys. 21* (Jan 1949), 44–48.

[25] Hapgood, M. Towards a scientific understanding of the risk from extreme space weather. *Advances in Space Research 47*, 12 (2011), 2059–2072. Recent Advances in Space Weather Monitoring, Modelling, and Forecasting - 2.

[26] Hayakawa, H., Ebihara, Y., Mishev, A., et al. The solar and geomagnetic storms in may 2024. *arXiv preprint* (2024).

[27] Heck, D., Capdeville, G. N., Knapp, J., et al. Corsika: A monte carlo code to simulate extensive air showers. Report FZKA 6019, Forschungszentrum Karlsruhe, 1998.

[28] Jil, A., Asvestari, E., Mishev, A., et al. New anisotropic cosmic-ray enhancement (acre) event on 5 november 2023 due to complex heliospheric conditions. *Solar Physics 299* (2024), 97.

[29] Karapetyan, T., Chilingarian, A., Hovsepyan, G., et al. The forbush decrease observed by the sevan particle detector network in the 25th solar activity cycle. *Journal of Atmospheric and Solar-Terrestrial Physics 262* (2024), 106305.

[30] Kudela, K., Bučík, R., and Bobík, P. On transmissivity of low energy cosmic rays in the disturbed magnetosphere. *Advances in Space Research 42* (2008), 1300.

[31] Kuwabara, T., Bieber, J. W., Clem, J., Evenson, P., Pyle, R., Munakata, K., Yasue, S., Kato, C., Akahane, S., Koyama, M., Fujii, Z., Duldig, M. L., Humble, J. E., Silva, M. R., Trivedi, N. B., Gonzalez, W. D., and Schuch, N. J. Real-time cosmic ray monitoring system for space weather. *Space Weather 4*, 8 (2006).

[32] Lockwood, J. A., Debrunner, H., and Flückiger, E. O. Indications for diffusive coronal shock acceleration of protons in selected solar cosmic ray events. *Journal of Geophysical Research 95*, A4 (1990), 4187–4201.

[33] Mavromichalaki, H., Papaioannou, A., Plainaki, C., et al. Applications and usage of the real-time neutron monitor database for solar particle events monitoring. *Advances in Space Research 47* (2011), 2210.

[34] Mishev, Alexander, and Usoskin, Ilya. Current status and possible extension of the global neutron monitor network. *J. Space Weather Space Clim. 10* (2020), 17.

[35] Moraal, H., Belov, A., and Clem, J. M. Design and co-ordination of multistation international neutron monitor networks. *Space Science Reviews 93* (2000), 285.

[36] Muangha, P., Ruffolo, D., Sáiz, A., et al. Variations in the inferred cosmic-ray spectral index as measured by neutron monitors in antarctica. *The Astrophysical Journal 974* (2024), 284.

[37] Munakata, K., Bieber, J. W., Yasue, S., et al. Precursors of geomagnetic storms observed by the muon detector network. *Journal of Geophysical Research 105*, A12 (2000), 27457–27468.

[38] Munakata, K., Hayashi, Y., Kozaiet, M., et al. Global analysis of the extended decreases in cosmic rays observed with worldwide networks of neutron monitors and muon detectors: Temporal variation of the rigidity spectrum and its implication. *The Astrophysical Journal 974* (2024), 283.

[39] Muraki, Y., Sakakibara, S., Shibata, S., Satoh, M., Murakami, K., Takahashi, K., Pyle, K. R., Sakai, T., and Mitsui, K. New solar neutron detector and large solar flare events of june 4th and 6th, 1991. *Journal of geomagnetism and geoelectricity 47*, 11 (1995), 1073–1078.

[40] Nelson, W., and Namito, Y. The egs4 code system: solution of gamma-ray and electron transport problems. Technical Report 5193, SLAC, 1990.

[41] Poluianov, S., and Batalla, O. Cosmic-ray atmospheric cutoff energies of polar neutron monitors. *Advances in Space Research 70*, 9 (2022), 2610–2617. Astrophysics of Cosmic Rays.

[42] Poluianov, S. V., Usoskin, I. G., Mishev, A. L., Moraal, H., Shea, M. A., and Smart, D. F. Gle and sub-gle redefinition in the light of high-altitude polar neutron monitors. *Solar Physics 292* (2017), 176.

[43] Raghav, A., Tari, P., Ghag, K., et al. The role of extreme geomagnetic storms in the forbush decrease profile. *arXiv preprint* (2021).

[44] Reames, D. V. *Solar Energetic Particles: A Modern Primer on Understanding Sources, Acceleration and Propagation*, vol. 978 of *Lecture Notes in Physics*. Springer, Cham, 2017.

[45] SIMPSON, J. Cosmic-radiation neutron intensity monitor. In *Geomagnetism*, International Council of Scientific Unions Comité Spécial de l'Année Géophysique Internationale (CSAGI), Ed., vol. 4 of *Annals of The International Geophysical Year*. Pergamon, 2013, pp. 351–373.

[46] Smart, D., and Shea, M. Fifty years of progress in geomagnetic cutoff rigidity determinations. *Advances in Space Research 44*, 10 (2009), 1107–1123. Cosmic Rays From Past to Present.

[47] Smith, A. W., Forsyth, C., Rae, I. J., Rodger, C. J., and Freeman, M. P. The impact of sudden commencements on ground magnetic field variability: Immediate and delayed consequences. *Space Weather 19* (2021), e2021SW002764.

[48] Soghomonyan, S., Chilingarian, A., and Pokhsraryan, D. Extensive air shower (eas) registration by the measurements of the multiplicity of neutron monitor signal, 2021.

[49] Stenkin, Y. V., Djappuev, D. D., and Valdés-Galicia, J. F. Neutrons in extensive air showers. *Yadernaya Fizika 70* (2007), 1123.

[50] Zazyan, M., and Chilingarian, A. Calculations of the sensitivity of the particle detectors of asec and sevan networks to galactic and solar cosmic rays. *Astroparticle Physics 32*, 3 (2009), 185–192.